Fluctuation and Noise Letters
Vol. 19, No. 3 (2020) 2050027 (16 pages)

DOI: 10.1142/S0219477520500273

Signal-to-Noise Ratio Estimation in Electromyography Signals Contaminated with Electrocardiography Signals

Thandar Oo and Pornchai Phukpattaranont*

Department of Electrical Engineering
Faculty of Engineering, Prince of Songkla University
Hat Yai, Songkhla 90112, Thailand
**pornchai.p@psu.ac.th*

Received 11 April 2019
Accepted 2 January 2020
Published 17 February 2020

Communicated by Marcin Kostur

When electromyography (EMG) signals are collected from muscles in the torso, they can be perturbed by the electrocardiography (ECG) signals from heart activity. In this paper, we present a novel signal-to-noise ratio (SNR) estimate for an EMG signal contaminated by an ECG signal. We use six features that are popular in assessing EMG signals, namely skewness, kurtosis, mean average value, waveform length, zero crossing and mean frequency. The features were calculated from the raw EMG signals and the detail coefficients of the discrete stationary wavelet transform. Then, these features are used as inputs to a neural network that outputs the estimate of SNR. While we used simulated EMG signals artificially contaminated with simulated ECG signals as the training data, the testing was done with simulated EMG signals artificially contaminated with real ECG signals. The results showed that the waveform length determined with raw EMG signals was the best feature for estimating SNR. It gave the highest average correlation coefficient of 0.9663. These results suggest that the waveform length could be deployed not only in EMG recognition systems but also in EMG signal quality measurements when the EMG signals are contaminated by ECG interference.

Keywords: Electromyography (EMG); Electrocardiography (ECG); signal-to-noise ratio (SNR); EMG pattern recognition.

1. Introduction

An accurate estimate of the signal-to-noise ratio (SNR) is of interest in a wide variety of contexts, including signal detection and estimation [1], machine learning [2] and image restoration [3]. SNR estimation algorithms are necessary and affect optimal performance in these contexts. For example, in [4], an SNR estimate was employed in a Wiener filter to suppress involuntary background spikes contaminating voluntary

*Corresponding author.

surface electromyography (EMG) signals. In this paper, we propose a novel algorithm for estimating the SNR of an EMG signal contaminated by electrocardiography (ECG) interference.

The EMG signal records electrical currents generated from contractions of skeletal muscles transmitted as electrical signals by motor units from the nerve-muscle functional unit of the neuromuscular system. The electrical potential difference can be measured either by non-invasive electrodes as surface EMG signals or by invasive needle electrodes as intramuscular EMG signals [5]. The electrodes convert an ion current to an electron current before amplifying and logging the signals. The EMG signal recorded from a muscle contraction has a variety of uses in clinical applications [6], robotic applications [7], modern human–computer interactions [8] and hand prosthesis control [9].

An EMG recognition system is essential to the performance of the mentioned applications. It consists of three cascaded modules, namely data pre-processing, feature extraction and classification [10]. The main objective of data pre-processing is to remove noise in the EMG signal, which is contaminated while passing through different tissues [11]. The EMG signal records the electrical potential difference across the skeletal muscle in every part of the body whereas the ECG signal measures the electrical potential difference across only the heart. However, when the EMG signal is collected from the muscles in the torso, it may be contaminated by the ECG signal coming from heart activity.

There are five techniques for removing ECG interference from the contaminated EMG signal: (1) linear filter [12, 13, 15, 16]; (2) template subtraction [12–14]; (3) adaptive filters including linear [12, 14, 19, 20] and nonlinear [12, 18–21] types; (4) wavelet transform [12, 17]; and (5) combined techniques, such as template subtraction combined with a high-pass filter [13], artificial neural network (NN) combined with wavelet transform [18] and adaptive neuro-fuzzy inference system combined with wavelet transform [14].

While many previous publications have focused on noise removal techniques, studies on SNR estimation remain rare. The EMG signal quality, which could be measured using SNR, is also of fundamental importance for achieving good performance in an EMG recognition system. In this paper, we develop an algorithm for estimating the SNR of an EMG signal contaminated by ECG interference based on both the raw EMG signal and its decomposition with discrete stationary wavelet transform (DSWT). The proposed method employs the features determined from the contaminated EMG signal as inputs to an NN for estimating SNR, which is the output of the NN.

The rest of this paper is organized as follows. Section 2 gives the necessary background on feature calculation, DSWT and NN. Section 3 describes the methods for signal generation, feature evaluation and the proposed SNR estimation algorithm. Results and discussion are provided in Secs. 4 and 5, respectively. Finally, we draw conclusions in Sec. 6.

2. Background

In this section, we describe three topics that are an important background for the proposed SNR estimation algorithm, consisting of feature calculation, DSWT and NN. These details are as follows.

2.1. *Feature calculation*

Feature calculation plays a vital role in improving the performance of the EMG signal recognition system. It is not only a process for reducing the dimensionality of the EMG signals, but is also useful in extracting significant information. In this paper, six popular features used in EMG signal recognition are employed in estimating the SNR, namely skewness (SKEW), kurtosis (KURT), mean absolute value (MAV), waveform length (WL), zero crossing (ZC) and mean frequency (MNF). While SKEW and KURT are common statistics, MAV and WL represent amplitude-based features. Besides, ZC and MNF are frequency-based features. Briefly, the details of each feature calculation are as follows:

- SKEW is a measure of asymmetry in probability distribution from EMG amplitudes. It is given by [22]

$$\text{SKEW} = \frac{\frac{1}{N}\sum_{i=1}^{N} x_i^3}{\left(\sqrt{\frac{1}{N}\sum_{i=1}^{N} x_i^2}\right)^3}, \tag{1}$$

  where x_i is the normalized EMG amplitude and N is the total number of EMG samples under calculation.
- KURT is used to measure the tail characteristic of the probability distribution from the EMG amplitudes. It can be expressed as [22]

$$\text{KURT} = \left[\frac{\frac{1}{N}\sum_{i=1}^{N} x_i^4}{\left(\frac{1}{N}\sum_{i=1}^{N} x_i^2\right)^2}\right] - 3. \tag{2}$$

- MAV is one of the most popular features and is widely used in the analysis of EMG signals. MAV is the average of the absolute values of EMG amplitudes in a sampled segment. It can be expressed as [10]

$$\text{MAV} = \frac{1}{N}\sum_{i=1}^{N} |x_i|. \tag{3}$$

- Wavelength (WL) is an indicator of the complexity of the EMG signal, representing the increase in the length of the EMG waveform over a time segment, and can be expressed as [10]

$$\text{WL} = \sum_{i=1}^{N-1} |x_{i+1} - x_i|. \tag{4}$$

- ZC quantifies the frequency information in the EMG signal. It is defined as the number of times that the EMG amplitudes pass through the zero level. We can add

a threshold T to prevent corruption by low voltage fluctuations or background noise. The ZC is described by [10]

$$\mathrm{ZC} = \sum_{i=1}^{N-1} [f(x_i \times x_{i+1}) \quad \text{and} \quad |x_i - x_{i+1}| \geq T], \tag{5}$$

where $f(x) = \begin{cases} 1, & \text{if } x < 0 \\ 0, & \text{otherwise} \end{cases}$.

- MNF is the sum of the product of the EMG power spectrum and the frequency divided by the total spectrum intensity. It is also known as the average frequency, as the center frequency, or as the spectral center of gravity [10]. It is given by [10, 29]

$$\mathrm{MNF} = \sum_{j=1}^{M} f_j P_j \Bigg/ \sum_{j=1}^{M} P_j, \tag{6}$$

where f_j is the frequency of the spectrum at frequency bin j, P_j is the EMG power spectrum at frequency bin j and M is the number of frequency bins.

2.2. *DSWT*

DSWT is known for its two crucial properties, time invariance and Gibbs phenomenon suppression. It can be used in a noise removal algorithm, as described in [23]. Therefore, the DSWT may replace a discrete wavelet transform (DWT) in some applications. DSWT can be performed by removing the up and down-samplers in DWT and modifying the filters with upsampling the coefficients from the previous decomposition level. As a result, the DSWT has the same number of samples between the input and the output at each decomposition level.

Let $x[n]$ be a signal and decompose it using L-level DSWT, as shown in Fig. 1. In the first-level decomposition, the two outputs are cA1, which is the set of approximation coefficients generated by convolving a low-pass filter $h_1[n]$ with the input signal $x[n]$ and cD1, which is the vector of detail coefficients generated by convolving a high-pass filter $g_1[n]$ with the input signal $x[n]$. It can be noted that the lengths of these two outputs, cA1 and cD1, are the same as that of $x[n]$.

In the second-level decomposition, the approximation coefficients, cA1, are used as an input signal to the filters $h_2[n]$ and $g_2[n]$, which are formed by upsampling the

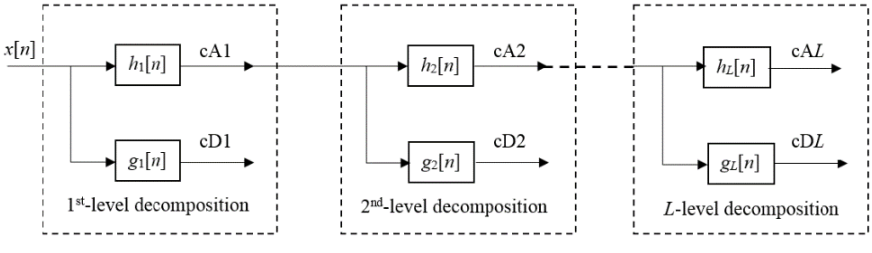

Fig. 1. L-level DSWT decomposition.

filters $h_1[n]$ and $g_1[n]$, respectively. Subsequently, we obtain two outputs for the second-level decomposition, namely cA2 and cD2 resulting from convolutions of cA1 with $h_2[n]$ and $g_2[n]$, respectively. These operations are repeated until the decomposition level L is reached.

In this paper, we calculated the features from DSWT decomposition ($L = 5$) and compared their performance in SNR estimate with those from the raw EMG signals. The cD4 and cD5 coefficients were of interest in this study because their frequency bands were 31.25–62.5 and 15.625–31.25 Hz, respectively, corresponded to the dominant frequency of the ECG signal. Moreover, the filters $h_i[n]$ and $g_i[n]$ were implemented based on the Symlet wavelet function, as suggested by [12].

2.3. *Neural network*

Neural networks (NN) have been successful in a variety of applications, such as speech recognition [24], image analysis [25] and adaptive control [26]. In this paper, an NN was used to estimate the SNR from the features described in Sec. 2.1. We used a two-layer feedforward network with a sigmoid transfer function in the hidden layer and a linear transfer function in the output layer. Levenberg–Marquardt optimization was used to update the weight and bias values of the network nodes in training. We evaluated the performance using a correlation coefficient (CC) of the SNR targets and the SNR estimates from NN, which can be expressed as [13, 14, 27]

$$\mathrm{CC} = \frac{\sum_{i=1}^{N}(s_t(i) - \bar{s}_t)(s_e(i) - \bar{s}_e)}{\sqrt{\sum_{i=1}^{N}(s_t(i) - \bar{s}_t)^2}\sqrt{\sum_{i=1}^{N}(s_e(i) - \bar{s}_e)^2}}, \tag{7}$$

where s_t is the true SNR and s_e is the estimate. A perfect linear relationship would be shown by $\mathrm{CC} = 1$, while $\mathrm{CC} = 0$ indicates random relationship (i.e., no association).

3. Materials and Methods

Three subtopics, namely signal generation, feature evaluation and SNR estimation, are discussed. In the signal generation subsection, we describe the methods used to generate the simulated EMG, simulated ECG and real ECG signals. Then, the methods used to evaluate features for an optimal SNR estimate are described. Finally, the proposed SNR estimate and its performance evaluation are given in the SNR estimation subsection.

3.1. *Signal generation*

3.1.1. *Simulated EMG signals*

We generated a simulated EMG signal from white Gaussian noise for the length of 2000 samples as an input to a band-pass filter with the frequency response [27]

$$H(f) = \frac{jf_U^2 f}{(f_L + jf)(f_U + jf)^2}, \tag{8}$$

where f_L was random between 30–60 Hz, $f_U = f_L + c$ and c was random between 30–100 Hz. The length of the simulated EMG signal matches 2 s of sampling at 1000 Hz. The total number of simulated EMG signals generated was 400.

3.1.2. *Simulated ECG signals*

A simulated ECG signal is generated by using three coupled ordinary differential equations as a dynamical model given by [28]

$$\dot{x} = \alpha x - \omega y, \tag{9}$$

$$\dot{y} = \alpha y + \omega x, \tag{10}$$

$$z = -\sum_{i \in \{P,Q,R,S,T\}} a_i \Delta\theta_i \exp\left(-\frac{\Delta\theta_i^2}{2b_i^2}\right) - (z - z_0), \tag{11}$$

where $\alpha = 1 - \sqrt{x^2 + y^2}$, $\Delta\theta_i = (\theta - \theta_i) \bmod 2\pi$, $\theta = \text{atan2}(y, x)$ (the four-quadrant arctangent of the real parts of the elements of x and y, with $-\pi \leq \text{atan2}(y, x) \leq \pi$) and ω is the angular velocity of the trajectory as it moves around the limit cycle. The parameters θ_i, a_i and b_i for the PQRST points were suggested by visualization of ECG from a normal subject. Table 1 gives the values of these three parameters used in the simulation. The sampling frequency for the simulated ECG signal was 256 Hz. The mean heart rate is random in the range of 60–100 beats per minute.

3.1.3. *Real ECG signals*

We used real ECG signals from the MIT-BIH arrhythmia database by segmenting a normal ECG beat from 40 out of 48 records. The length of each segmented signal was 20 s. We resampled each segment from 360 Hz to 1000 Hz so that it aligned with the sampling rate of the EMG signal. Finally, we divided each 20 s data into 10 2 s segments. As a result, the total number of segmented real ECG signals was 400. Figure 2 shows an example of simulated and real ECG signals in the time domain (top panel) and their power spectra in the frequency domain (bottom panel).

3.2. *Feature evaluation*

We describe the method used for evaluating features in this section. Firstly, we generated the EMG signals contaminated with ECG interference at 5 SNR levels from −20 dB to 0 dB with a step size of 5. The SNR range [−20, 0] dB was of interest because we obtained an excellent detection on the type of noise when the SNR is

Table 1. Specific parameters used for generating simulated ECG.

Parameter	Description	P	Q	R	S	T
θ_i (degrees)	Angles of extrema	−70	−15	0	15	100
a_i	z-position of extrema	1.2	−5.0	30.0	−7.5	0.75
b_i	Gaussian width of peaks	0.25	0.1	0.1	0.1	0.4

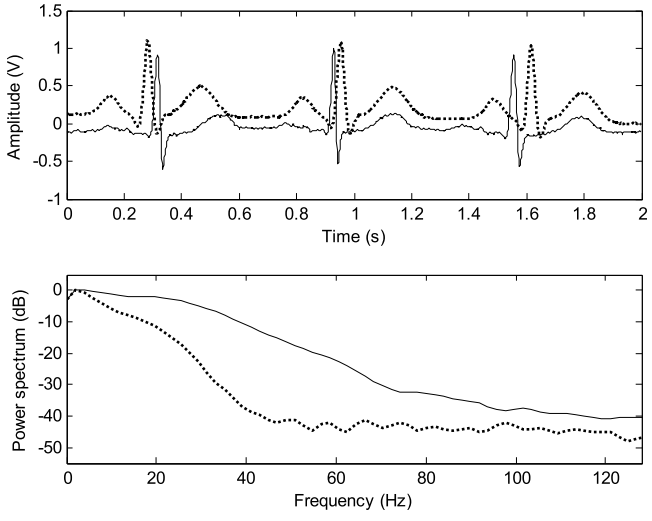

Fig. 2. Examples of simulated (dotted line) and real (solid line) ECG signals in the time domain (top panel) and their power spectra in the frequency domain (bottom panel). The mean heart rate for the simulated ECG signal is 90 beats per minute.

below 0 dB [27]. After the type of noise was known, SNR was estimated with the algorithm that was appropriate to detect this type of noise. The dataset contained simulated EMG signals contaminated with the real ECG signal. Fifty real ECG signals were randomly chosen and were amplitude scaled with 50 simulated EMG signals at each SNR level. The SNR was calculated from

$$\mathrm{SNR} = 10 \log_{10}\left(\frac{P_x}{P_n}\right), \tag{12}$$

where P_x is the average power of the EMG signal and P_n is the average power of the ECG signal.

Secondly, after the contaminated EMG signal was generated, it was normalized by

$$x_j = \frac{x_k - \bar{x}}{S}, \tag{13}$$

where x_k is the EMG amplitude, $\bar{x}$ is the mean and S is the standard deviation. Then, x_j was normalized to have unit energy, as described by

$$x_i = \frac{x_j}{\sqrt{\sum_{i=1}^{N} x_j^2}}, \tag{14}$$

where N is the length of the signal. Subsequently, the cD4 and cD5 coefficients were determined for the normalized EMG signals x_i.

Finally, we generated six features, namely, SKEW, KURT, MAV, WL, ZC, and MNF, for the 50 normalized contaminated EMG signals, and cD4 and cD5

coefficients for each SNR level. Boxplots of each feature for the five SNR levels were used in the evaluation.

3.3. *SNR estimation*

3.3.1. *Training and testing data preparation*

The EMG signals contaminated with ECG interference were generated using uniformly random SNR in the range [−20, 0] dB. Subsequently, we generated two datasets. The first dataset had simulated EMG signals contaminated with simulated ECG interference. The second dataset had simulated EMG signals contaminated with real ECG interference. Details of generating each dataset are as follows.

- Simulated EMG contaminated with simulated ECG (SMSC): Three hundred pairs of simulated ECG and EMG signals were randomly selected. Then, each pair was combined with amplitude scaling to obtain a chosen SNR level, which was a uniformly distributed random number between −20 and 0. This dataset was used in the training step.
- Simulated EMG contaminated with real ECG (SMRC): This dataset has the same generating process as the SMSC dataset, except for substituting the simulated ECG signals with the real ECG signals. One hundred simulated EMG signals and 100 real ECG signals were randomly chosen. Subsequently, they were combined to achieve the SNR range [−20 0] dB with a uniform random distribution. This dataset was used in the testing step.

After EMG contamination, we normalize signals and calculate features from both SMSC and SMRC dataset using the method described in Sec. 3.2.

3.3.2. *SNR estimation algorithm*

The proposed method for estimating SNR consists of six main stages. Details on each stage are as follows.

- Stage (1) Normalize each feature from the SMSC dataset by

$$z = \frac{f - \mu}{\sigma}, \tag{15}$$

  where f is a feature, μ and σ are the mean and standard deviation of each feature, respectively.
- Stage (2) Train NN with the normalized features from Stage (1). The input vectors and target vectors will be randomly divided into three sets as follows: 70% will be used for training, 15% will be used to validate that the network is generalizing and to stop training before overfitting. The last 15% will be used as a completely independent test of generalization. The number of hidden neurons is 20.
- Stage (3) Normalize each feature from the SMRC dataset using Eq. (15) and use them as the testing data.

- Stage (4) Apply the trained NN from Stage (2) to the testing data from Stage (3).
- Stage (5) Evaluate performance between the SNR target and the estimated SNR from NN using CC.
- Stage (6) Repeat Stages (1)–(5) five times using newly-generated SMSC and SMRC data. Evaluate the performance of the proposed algorithm using the mean and standard deviation from five CC values.

4. Results

4.1. *Feature evaluation*

We extracted six features for the contaminated EMG signals at five SNR levels, generated as described in Sec. 3.2. Figure 3 shows boxplots of the six features for SMRC data by SNR level. Figure 3(a) shows the boxplots of SKEW from raw, cD4 and cD5 data in the top, middle and bottom panels, respectively. Figures 3(b)–3(f) show similar boxplots of the other five features, namely KURT, MAV, WL, ZC and MNF. The WL feature for the raw EMG data gives the best separation, as seen in the

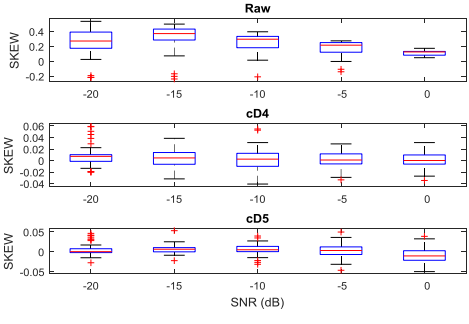

(a) SKEW

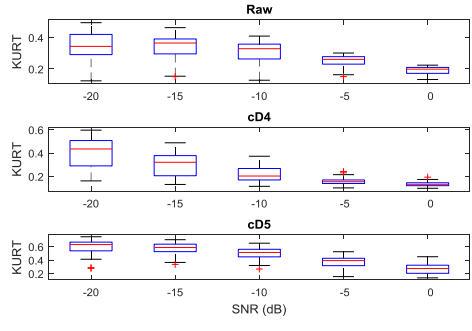

(b) KURT

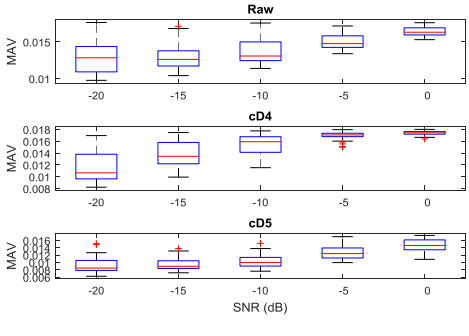

(c) MAV

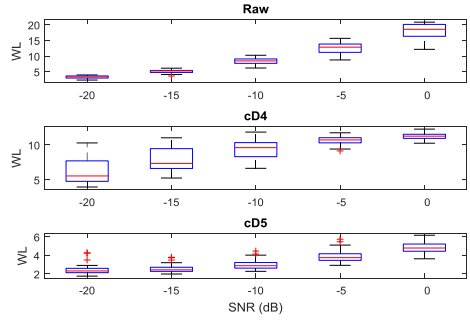

(d) WL

Fig. 3. Boxplots of feature values determined using the SMRC data as a function of SNR. (a) SKEW, (b) KURT, (c) MAV, (d) WL, (e) ZC and (f) MNF.

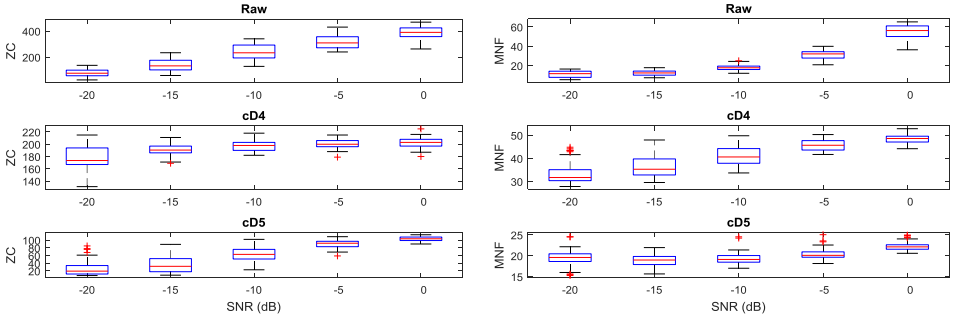

(e) ZC (f) MNF

Fig. 3. (*Continued*)

top panel of Fig. 3(d). However, the SKEW features from cD4 and cD5 decomposition levels do not give good separation, as seen in Fig. 3(a).

4.2. *SNR estimation*

We implemented the SNR estimation algorithm as described in Sec. 3.3 and demonstrated the performance of SNR estimation for a single feature and paired features using CC in Tables 2 and 3, respectively. Table 2 shows the mean and standard deviation for CC from different single features obtained for the SMRC data when these six features are calculated using raw, cD4 and cD5 EMG data. We can see that the WL feature from the raw EMG data gives the best average CC at 0.9663. The best average CCs from cD4 and cD5 are 0.7738 and 0.8359, respectively. These results show that SNR estimates for EMG signals contaminated with ECG interference using the raw EMG data are better than with DSWT data. Table 3 shows the mean and standard deviation of CC from different pairs of features for the SMRC data. We can see that the combination of WL and MNF (WL+MNF) for the raw EMG data gives the best average CC at 0.9566. Figure 4 shows an example of the correlation plot for the SNR estimate from NN with the WL feature from the raw EMG data. The CC of 0.9784 agrees well with the results from the WL feature using the raw data (0.9663 ± 0.0085) shown in Table 2.

Table 2. Mean and standard deviation of CC from single features for the SMRC data.

Features	Raw	cD4	cD5
SKEW	0.5541 ± 0.0754	-0.0896 ± 0.0935	0.2054 ± 0.1834
KURT	0.6400 ± 0.0409	0.6982 ± 0.0877	0.7678 ± 0.0162
MAV	0.4903 ± 0.1109	0.7152 ± 0.0244	0.7137 ± 0.0219
WL	0.9663 ± 0.0085	0.7738 ± 0.0244	0.8264 ± 0.0282
ZC	0.8321 ± 0.0358	0.5064 ± 0.0602	0.8359 ± 0.0208
MNF	0.9146 ± 0.0296	0.7114 ± 0.0858	0.5247 ± 0.0679

Table 3. Mean and standard deviation of CC with pairs of features for the SMRC data.

Feature pair	Raw	cD4	cD5
SKEW+KURT	0.3765 ± 0.1037	0.5980 ± 0.1137	0.7398 ± 0.0573
SKEW+WL	0.7591 ± 0.2312	0.6599 ± 0.0518	0.8295 ± 0.0374
SKEW+ZC	0.7686 ± 0.0848	0.3412 ± 0.0292	0.7966 ± 0.0833
SKEW+MAV	0.3903 ± 0.1008	0.5491 ± 0.1365	0.6882 ± 0.0475
SKEW+MNF	0.7743 ± 0.0894	0.7103 ± 0.0545	0.5002 ± 0.0312
KURT+WL	0.9475 ± 0.0261	0.7192 ± 0.0353	0.8649 ± 0.0281
KURT+ZC	0.8822 ± 0.0329	0.6907 ± 0.0673	0.8005 ± 0.0278
KURT+MAV	0.5172 ± 0.0533	0.6732 ± 0.0508	0.7083 ± 0.0327
KURT+MNF	0.8844 ± 0.0364	0.7385 ± 0.0414	0.7211 ± 0.0685
WL+ZC	0.8837 ± 0.0470	0.7177 ± 0.0473	0.8382 ± 0.0248
WL+MAV	0.9144 ± 0.0392	0.7235 ± 0.0458	0.8586 ± 0.0184
WL+MNF	0.9566 ± 0.0097	0.6953 ± 0.0821	0.7251 ± 0.0841
ZC+MAV	0.8597 ± 0.0417	0.6994 ± 0.0549	0.7936 ± 0.0229
ZC+MNF	0.9272 ± 0.0229	0.7158 ± 0.0517	0.7610 ± 0.1661
MAV+MNF	0.8517 ± 0.0870	0.7331 ± 0.0392	0.5857 ± 0.1108

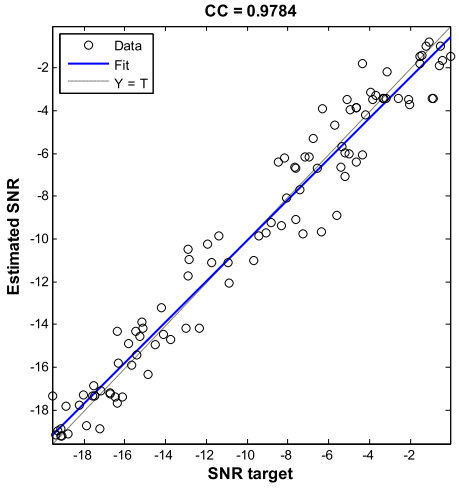

Fig. 4. Correlation of SNR target and its estimate from a trained NN when the input is the WL features for the SMRC dataset.

5. Discussion

In this section, we assess the results in Sec. 4 for further insights. Figure 5 (left column) shows the raw, cD4 and cD5 EMG data in SMRC, respectively. Figure 5 (right column) shows the corresponding absolute differences of two adjacent amplitudes from the signals in the left column. It is evident that the absolute differences of two adjacent amplitudes from the WL feature for the raw EMG and cD5 data are better than those for the cD4 data. As a result, the average CC value from

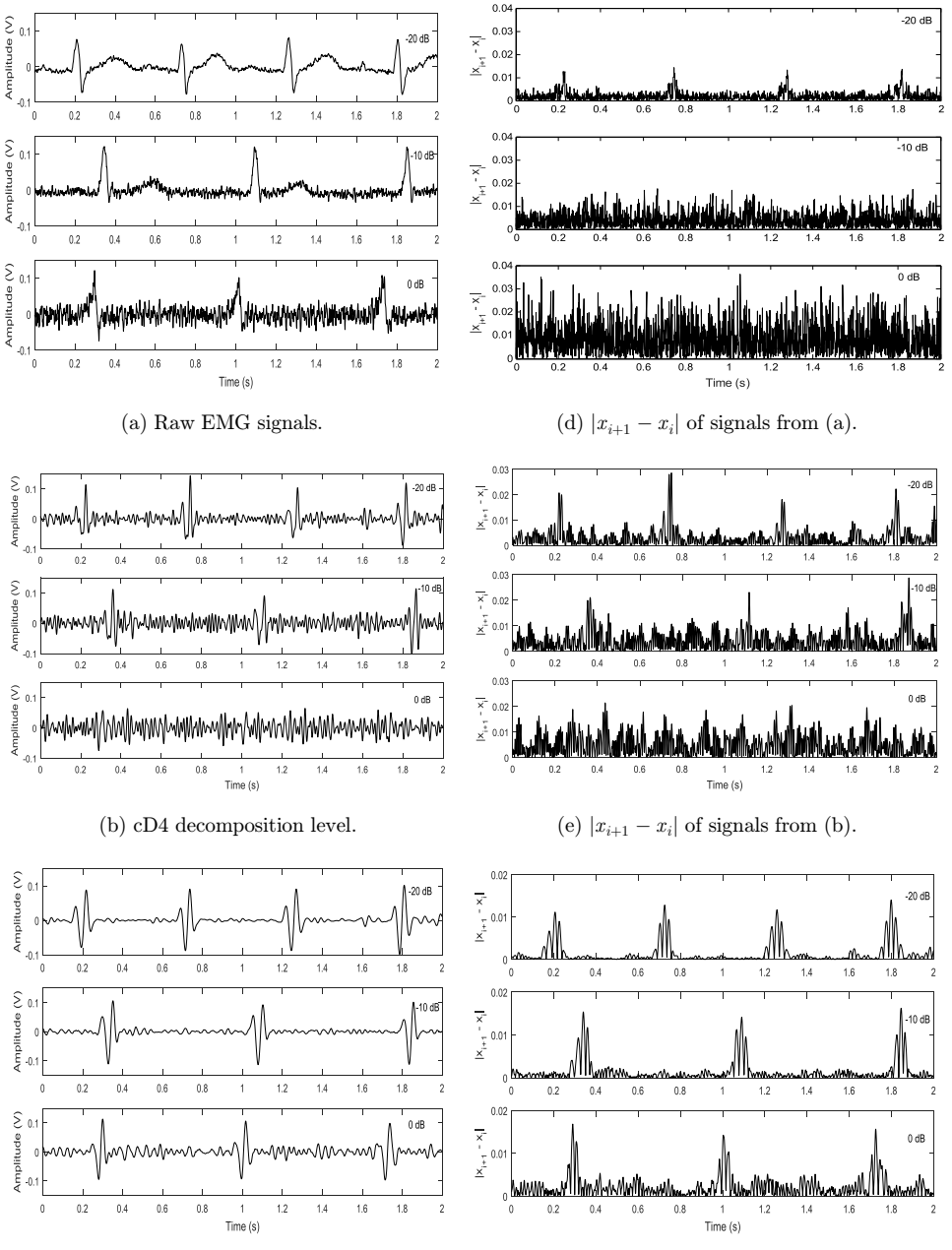

(a) Raw EMG signals.

(d) $|x_{i+1} - x_i|$ of signals from (a).

(b) cD4 decomposition level.

(e) $|x_{i+1} - x_i|$ of signals from (b).

(c) cD5 decomposition level.

(f) $|x_{i+1} - x_i|$ of signals from (c).

Fig. 5. Example of the SMRC signals and their absolute differences of adjacent amplitudes ($|x_{i+1} - x_i|$) are shown in the left and right columns, respectively. The top, middle and bottom rows show the results for raw EMG signals, cD4 decomposition level and cD5 decomposition level, respectively.

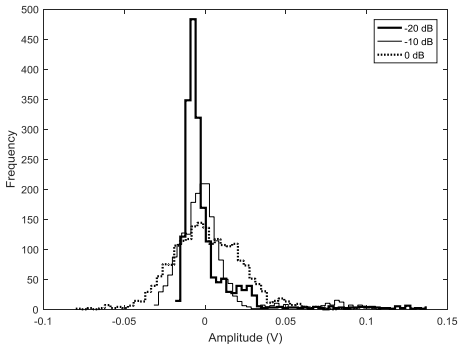

(a) Histograms for raw EMG signals.

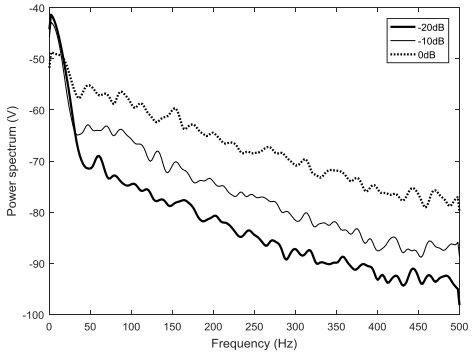

(d) Power spectra for raw EMG signals.

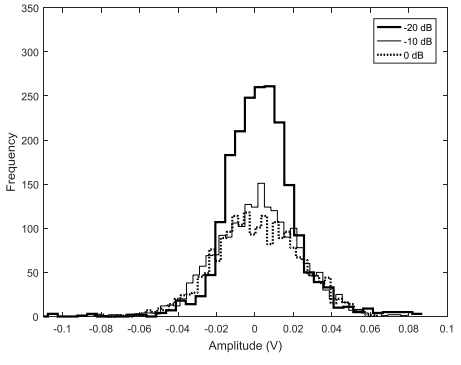

(b) Histograms for cD4 decomposition level.

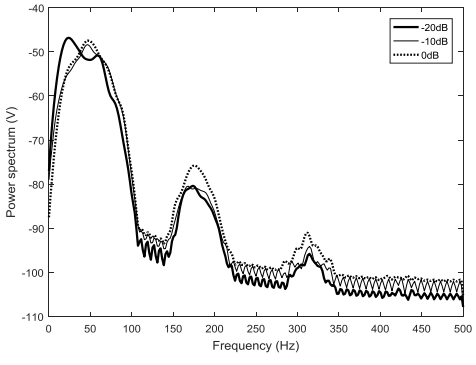

(e) Power spectra for cD4 decomposition level.

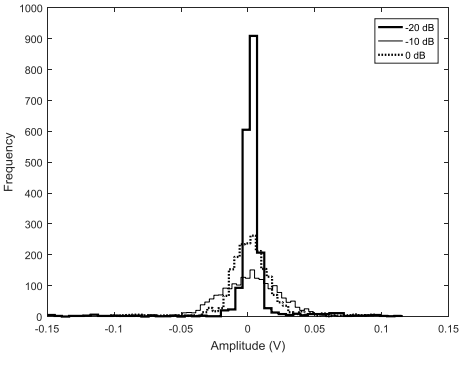

(c) Histograms for cD5 decomposition level.

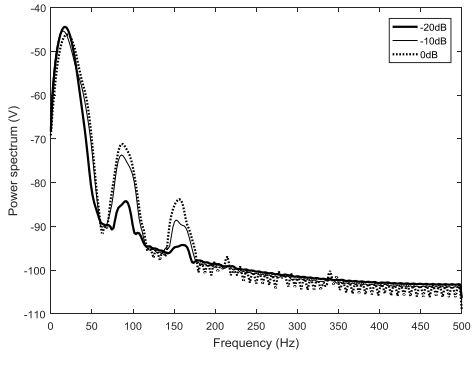

(f) Power spectra for cD5 decomposition level.

Fig. 6. Histograms and power spectra for the SMRC data are shown in the left and right columns, respectively. The top, middle and bottom rows show the results for raw EMG signals, cD4 decomposition level and cD5 decomposition level, respectively.

WL using the raw EMG data provides the best result at 0.9663 compared to that from cD4 at 0.7738 and cD5 at 0.8264. Moreover, these results are in agreement with the boxplots shown in Fig. 3(d).

We can gain more insight into SKEW and KURT from histograms. Figure 6 (left column) shows histograms from raw, cD4 and cD5 in the top, middle and bottom rows, respectively. We can see that the histograms from the cD4 and cD5 data are more symmetric than those from the raw EMG data. As a result, the SKEW values are more overlapped. These results agree with the boxplot of SKEW values by the 5 SNR levels shown in Fig. 3(a). Also, they agree with the average CC values. In other words, the raw EMG data give better average CC (0.5541) than cD4 (−0.0896) and cD5 (0.2054) data when SKEW is used as a feature. However, the tailedness of histograms can be distinguished among raw, cD4 and cD5 EMG data when SNR increases. Therefore, the average CC values from KURT using raw, cD4 and cD5 data are comparable and better than those from SKEW at 0.6400, 0.6982 and 0.7678, respectively. These are also supported by the separations seen in the boxplots of Figs. 3(a)–3(b).

We can understand MNF better with power spectra. Figure 6 (right column) shows the power spectra for the raw, cD4 and cD5 EMG data in the top, middle and bottom rows, respectively. The power spectra from the raw EMG and cD4 data have better separation than those for the cD5 data as SNR increases. In other words, the cD5 data do not give a difference in MNF when SNRs increase because of the similarity in power spectra. Therefore, the average CC value from MNF using the raw EMG data gives the best result (0.9146) superior to those from MNF using the cD4 (0.7114) and cD5 (0.5247) data. Also, we can see that it has an excellent separation in the boxplots of Fig. 3(f).

6. Conclusions

We presented a method for estimating SNR in an EMG signal contaminated by ECG interference. The approach consisted of two main parts, namely feature evaluation and SNR estimation. We evaluated six features often used in EMG recognition systems, namely SKEW, KURT, MAV, WL, ZC and MNF. The features were calculated from the raw EMG signals and their corresponding cD4 and cD5 coefficients of DSWT. The results show that WL from the raw EMG signals gave the best performance. Subsequently, WL was used as an input to an NN for SNR estimation. While we used simulated EMG data artificially contaminated with simulated ECG data in the training stage, the simulated EMG data was artificially contaminated with real ECG data in the testing stage. The best average CC 0.9663 was obtained with WL as the input to the NN. There is no prior study about SNR estimation for an EMG signal contaminated with ECG interference. Therefore, in this paper, we demonstrated a novel method of SNR estimation for an EMG signal contaminated with ECG interference. The results suggest a possible future research direction

employing the SNR estimation algorithm to improve the performance of an EMG recognition system.

Acknowledgments

This work was supported by the Graduate School, Prince of Songkla University through Thailand's Education Hub for ASEAN Countries (TEH-AC) scholarship. Moreover, it was jointly funded by the Thailand Research Fund and Faculty of Engineering, Prince of Songkla University through Contract No. RSA6280016, in part by the Higher Education Research Promotion and National Research University Project of Thailand, Office of the Higher Education Commission. Also, the authors would like to thank the Research and Development Office (RDO), Prince of Songkla University and Associate Professor Dr. Seppo Karrila, Faculty of Science and Technology, Prince of Songkla University for commenting on this paper.

References

[1] M. Suliman, T. Ballal, A. Kammoun and T. Y. Al-Naffouri, Constrained perturbation regularization approach for signal estimation using random matrix theory, *IEEE Signal Process Lett.* **23** (2016) 1727–1731.

[2] D. J. Sebald and J. A. Bucklew, Support vector machine techniques for nonlinear equalization, *IEEE Trans. Signal Process* **48** (2000) 3217–3226.

[3] J. C. Pesquet, A. B. Benyahia and C. Chaux, A SURE approach for digital signal/image deconvolution problems, *IEEE Trans. Signal Process* **57** (2009) 4616–4632.

[4] J. Liu, D. Ying and P. Zhou, Wiener filtering of surface EMG with a priori SNR estimation toward myoelectric control for neurological injury patients, *Med. Eng. Phys.* **36** (2014) 1711–1715.

[5] D. Staudenmann, K. Roeleveld, D. F. Stegeman and J. H. V. Dieën, Methodological aspects of SEMG recordings for force estimation — A tutorial and review, *J. Electromyogr. Kines* **20** (2010) 375–387.

[6] B. Pandey and R. B. Mishra, A practical measuring system for intestinal pressure activity and its clinical application, *Expert Syst. Appl.* **36** (2009) 9201–9213.

[7] F. Christian, W. Andreas, K. Konstantin and H. Gunter, Application of EMG signals for controlling exoskeleton robots, *Biomed Tech (Berl)* **51** (2006) 314–319.

[8] A. Barreto, S. Scargle and M. Adjouadi, A practical EMG-based human-computer interface for users with motor disabilities, *J. Rehabil. Res. Dev.* **37** (2000) 53–64.

[9] K. Veer, Experimental study and characterization of SEMG signals for upper limbs, *Fluct. Noise Lett.* **14** (2015) 1550028.

[10] A. Phinyomark, P. Phukapattranont and C. Limsakul, Feature reduction and selection for EMG signal classification, *Expert Syst. Appl.* **39** (2012) 7420–7431.

[11] G. F. Inbar and A. E. Noujaim, On surface EMG spectral characterization and its application to diagnostic classification, *IEEE Trans. Biomed. Eng.* **31** (1984) 597–604.

[12] P. Zhou, Eliminating cardiac contamination from myoelectric control signals developed by targeted muscle reinnervation, *Physiol Meas.* **27** (2007) 1311–1327.

[13] J. D. M. Drake and J. P. Callagham, Elimination of electrocardiogram contamination from electromyogram signals, An evaluation of currently used removal techniques, *J. Electromyogr. Kines* **16** (2006) 175–187.

[14] S. Abbaspour, A. Fallah, M. Linden and H. Gholamhosseini, A novel approach for removing ECG interferences from surface EMG signals using a combined ANFIS and wavelet, *J. Electromyogr. Kines* **26** (2016) 52–59.
[15] R. Istenic, P. A. Kaplanis, C. S. Pattichis and D. Zazula, Analysis of neuromuscular disorders using statistical and entropy metrics on surface EMG, *WSEAS Trans Signal Process* **4** (2008) 1790–5052.
[16] S. Conforto, T. D'Alessio and S. Pignatelli, Optimal rejection of movement artifacts from myoelectric signals by means of a wavelet filtering procedure, *J. Electromyogr. Kines* **9** (1999) 47–57.
[17] M. Shahbakhti, E. Heydari and G. T. Luu, Segmentation of ECG from surface EMG using DWT and EMD: A comparison study, *Fluct. Noise Lett.* **13** (2014) 1450030.
[18] S. Abbaspour and A. Fallah, A combination method for electrocardiogram rejection from surface electromyogram, *Open Biomed. Eng. J.* **8** (2014) 13–19.
[19] C. Marque, C. Bisch, R. Dantas, S. Elayoubi, V. Brosse and C. Pérot, Adaptive filtering for ECG rejection from surface EMG recordings, *J. Electromyogr. Kines* **15** (2005) 310–315.
[20] G. Lu, J. S. Brittain, P. Holland, J. Yianni, A. L. Green, J. F. Stein, T. Z. Aziz and S. Wang, Removing ECG noise from surface EMG signals using adaptive filtering, *Neurosci. Lett.* **462** (2009) 14–19.
[21] C. K. S. Vijila and C. E. S. Kumar, Cancellation of ECG in electromyogram using back propagation network, *Proc. IEEE. T. Vis, Comput. Gr. Int. Conf.* 27–28 October 2009, Kottyam, Kerala, pp. 1–5.
[22] S. Thongpanja, A. Phinyomark, F. Quaine, Y. Laurillau, C. Limsakul and P. Phukpattaranont, Probability density functions of stationary surface EMG signals in noisy environments, *IEEE Trans. Instrum. Meas.* **65** (2016) 1547–1557.
[23] T. D. Bui and G. Chen, Translation-invariant denoising using multiwavelets, *IEEE Trans. Signal Process* **46** (1998) 3414–3420.
[24] S. Garimella, S. H. Mallidi and H. Hermansky, Regularized auto-associative neural networks for speaker verification, *IEEE Signal Process Lett.* **19** (2012) 841–844.
[25] S. E. Hussein, O. A. Hassan and M. H. Granat, Assessment of the potential iridology for diagnosing kidney disease using wavelet analysis and neural networks, *Biomed. Signal Process. Control* **8** (2013) 534–541.
[26] K. S. Narendra and S. Mukhopadhyay, Adaptive control using neural networks and approximate models, *IEEE Trans. Neural Netw.* **8** (1997) 475–485.
[27] P. McCool, G. D. Fraser, A. D. C. Chan, L. Petropoulakis and J. J. Soraghan, Identification of contaminant type in surface electromyography (EMG), *IEEE Trans. Neural Syst. Rehabil. Eng.* **22** (2014) 774–783.
[28] P. E. McSharry, G. D. Clifford, L. Tarassenko and L. A. Smith, A dynamical model for generating synthetic electrocardiogram signals, *IEEE Trans. Biomed. Eng.* **50** (2003) 289–294.
[29] G. D. Fraser, A. D. C. Chan, J. R. Green and D. T. Macisaac, Automated biosignal quality analysis for electromyography using a one-class support vector machine, *IEEE Trans. Instrum. Meas.* **63** (2014) 2919–2930.